Elaboration of capsules from Pickering double emulsion polymerization stabilized solely by cellulose nanocrystals

Hanaé Dupont, Valérie Héroguez, Véronique Schmitt

Elaboration of capsules from Pickering double emulsion polymerization stabilized solely by cellulose nanocrystals

Hanaé Dupont[1,2], Valérie Héroguez[2,*], Véronique Schmitt[1,*]

[1] Centre de Recherche Paul Pascal, UMR 5031 Univ. Bordeaux, CNRS, 115 avenue du Dr Albert Schweitzer, 33600 Pessac, France.

[2] Laboratoire de Chimie des Polymères Organiques, Univ. Bordeaux, CNRS, Bordeaux INP, UMR 5629, Bordeaux, 16 Avenue Pey-Berland, F-33607 Pessac, France.

* corresponding authors

veronique.schmitt@crpp.cnrs.fr

heroguez@enscbp.fr

Abstract

Pickering double oil-in-water-in-oil emulsions O/W/O were stabilized using solely cellulose nanocrystals (CNCs), which were modified by introducing surface brominated functions. The emulsions were formulated using only bio-friendly components, among which isopropyl myristate as oil phase, hydroxyl oligoethylene glycol methacrylate (OEGMA) as macromonomer, tetraethylene glycol diacrylate (TEGDA) as cross-linker, and CNCs as stabilizing particles. Formulation parameters could be tuned easily to modulate the fraction of inner emulsion droplets within the double emulsion drops or change the monomer(s) composition within the aqueous phase. The latter was further polymerized to synthesize matrix capsules. The obtained objects showed good resistance to the vacuum and were efficiently used as promising encapsulation vessels. Both hydrophobic and hydrophilic model dyes were encapsulated, with an encapsulation efficiency of about 90%.

Keywords: Pickering, cellulose, oil-in-water-in-oil, polymerization, encapsulation

1. Introduction

Emulsions are metastable systems and are defined as the mixture of at least two immiscible liquids. Therefore, their kinetic stabilization requires the use of stabilizing agents, like surfactants, polymers or particles. A rising interest has been put towards the use of particles and the study of the related Pickering emulsions to replace the widely used (macro)molecular scale surfactants (Arditty et al., 2004; Gonzalez Ortiz et al., 2020). Pickering emulsions were discovered by Pickering (Pickering, 1907) and Ramsden (Ramsden, 1904) in the early 1900's and have regained interest since the 2000's because of their high kinetic stability and ease of implementation. According to rising environmental and transparency concerns, the use of organic particles with natural origin as renewable and harmless stabilizers has been considered (Dupont, Maingret, et al., 2021; Sarkar & Dickinson, 2020). Among them, cellulose nanocrystals (CNCs) appear as particles with high potential because they are biosourced and highly available, they are biodegradable and they exhibit a well-known functionalized structure that offers an easily modifiable surface. Studies have shown that they efficiently stabilize direct oil-in-water (O/W) (Deng et al., 2018; Gestranius et al., 2017; Hedjazi & Razavi, 2018; Kalashnikova et al., 2011; Mackie et al., 2019) and inverse water-in-oil (W/O) (Dupont, Laurichesse et al, 2021 ; Guo et al., 2017; Lee et al., 2013; Zhang et al., 2018) Pickering emulsions. However, the occurrences in the literature of more complex systems such as multiple emulsions are still scarce. In most cases, only one of the two interfaces is stabilized by natural organic particles, the other being stabilized by surfactants. This was indeed the case in the study of Matos *et al.* (Matos et al., 2013) who used starch nanoparticles to stabilize the outer interface of water-in-oil-in-water (W/O/W) emulsions, along with a hydrophobic polyglycerol polyricinoleate (PGPR) for the inner interface. More recently, scarce studies reporting double emulsions stabilized solely by particles with natural origin were published. Spyropoulos *et al.* (Spyropoulos et al., 2019) showed good stability of W/O/W emulsions stabilized by rutin particles for the O/W interface, and nanocellulose for the W/O interface, and Cunha *et al.* (Cunha et al., 2014) formulated an O/W/O (oil-in-water-in-oil) emulsions fully stabilized by cellulose derivatives (CNC and/or CNF). Both works focused on the formulation

of the double emulsion system as a proof of concept, but did not used it for any particular application. The only example of application of such systems was demonstrated by Pan *et al.*, who used lignin particles to produce a W/O/W double emulsions, which intermediate phase was further polymerized to produced porous absorbent beads (Pan et al., 2015). Hence, we here propose to investigate further the potential of Pickering double emulsions stabilized solely with cellulose nanocrystals as polymeric vessels for encapsulation. CNCs of both interfaces were submitted to the same modification process, their modification rate being the only variable to modulate their wettability. In the present work, O/W Pickering emulsion was stabilized using hydrophilic CNCs. This direct emulsion was then used as dispersed phase for a second emulsification step to produce an O/W/O Pickering double emulsion stabilized by hydrophobic CNCs, using isopropyl myristate as a biocompatible oil phase. Based on a preliminary study conducted on W/O emulsions (Dupont, Laurichesse, et al., 2021), the intermediate aqueous phase of the double emulsion, composed of hydroxyl oligoethylene glycol methacrylate (OEGMA) and an potential cross-linker (tetraethylene glycol diacrylate, TEGDA), was subsequently polymerized by free radical polymerization to obtain solid capsules as schematically depicted in Figure 1. The resulting objects were further proven efficient encapsulation vessels for both hydrophobic and hydrophilic model dyes, showing the high applicative potential of these objects.
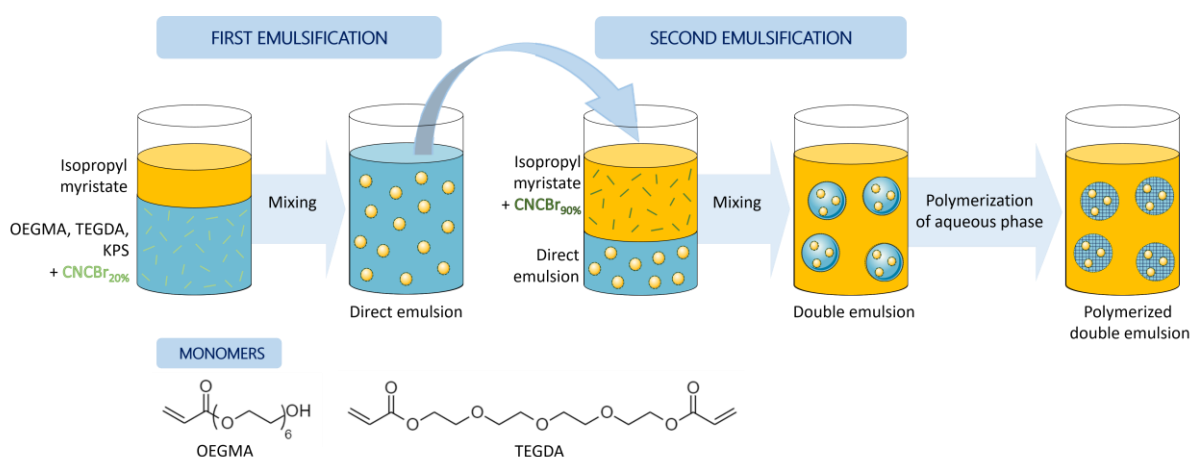
Figure 1: Principle scheme for the two-step emulsification and synthesis of the polymerized double O/W/O emulsions.

77 **2. Experimental**

78 **2.1 Materials**

79 Pristine CNCs were purchased from The University of Maine, under freeze-dried CNC form,

80 isolated from sulfuric acid hydrolysis of wood pulp. The crystals present initially on their surface

81 both sulfate (1.05 wt% as data from the provider) and hydroxyl functions (3.10 ± 0.11 mmol.g^{-1}

82 ^{1} of CNC). The initial CNCs exhibited a rod-like shape with estimated dimension of L=138 ± 47

83 nm in length and l=25 ± 6 nm in width based on AFM analysis (Dupont et al., 2020; Dupont,

84 Laurichesse, et al., 2021).

85 Triethylamine (TEA) (Fisher scientific, 99%), α-bromoisobutyryl bromide (Bibb) (ABCR, 98%),

86 dimethylaminopyridine (DMAP) (Sigma Aldrich, 99%) were used for the CNC modification

87 without any purification. Isopropyl myristate (IPM) (98%, Alfa Aesar), an oil allowed for

88 cosmetic applications, was used as received as the oil phase for all the emulsion systems.

89 Hydroxyl oligoethylene glycol methacrylate (OEGMA, M_n = 360 g/mol) (Sigma Aldrich),

90 tetraethylene glycol diacrylate (TEGDA) (Sigma Aldrich) were used as macromonomer and

91 cross-linker without purification. Potassium persulfate (KPS) (>99%, Sigma Aldrich) was used

92 as received. Fluorescent yellow (FY131SC) (Dow Chemicals) containing Solvent Red 175,

93 methylene blue (Fluka) and toluidine blue (Acros) were used as fluorescent dyes.

94 **2.2 CNC-Br synthesis**

95 CNC-Br synthesis was first described by Meng *et al.* (Meng et al., 2008) and Morandi *et al.*

96 (Morandi et al., 2009), modified by Werner *et al.* (Werner et al., 2019) and optimized in the

97 present work. 2 g of CNC and 2 g of DMAP were introduced in a double-wall reactor. After a

98 nitrogen purge, 100 mL of dry DMF were added to the powders under gentle agitation with a

99 magnetic stirrer. The solution was cooled down to 0°C. 8.5 g (1.48 mol/L) of Bibb (reactant)

100 and 4.8 g (1.90 mol/L) of TEA, were added to the solution under vigorous agitation. After 3 h

101 for the least modified and 41 h for the most modified, CNC-Br were precipitated in 200 mL of

102 a mixture of THF/ethanol (50/50$_{v/v}$), isolated by centrifugation (6000 rpm, 10 min, 15°C) and

103 redispersed in water. For a short modification time, that means a low modification rate (3 h,

104 particles noted CNC-Br$_{20\%}$), the aqueous suspension of CNC-Br was dialyzed against pure

105 water during 7 days with a 1 kDa membrane. For a long modification time, that means a high

106 modification rate (41 h, particles noted CNC-Br$_{90\%}$), the purification procedure was different.

107 THF was subsequently added to the CNC-Br aqueous dispersion before centrifugation, in a

108 ratio 1:1. This step was repeated at least 3 times to remove all unreacted species. For both

109 modification times, the final dispersion in water was freeze-dried to obtain a powder.

110 The grafting was confirmed by CP MAS NMR and FT-IR by following the appearance of the

111 stretching bonds corresponding to the surface ester groups at 1760 cm^{-1} (v(C=O)) and 1060

112 cm^{-1} (v(C-O)) (Fig. S1, SI). Quantitative evaluation of modification rates was determined by

113 elemental analysis thanks to the mass percentage of bromine and the amount of surface

114 hydroxyl groups (Eq. 1).

115 $$\% \ substitution = \frac{mmol \ of \ Br \ by \ gram \ of \ CNCs}{mmol \ of \ surface \ hydroxyl \ functions \ by \ gram \ of \ CNCs} = \frac{n_{Br}}{n_{OH}}.100 \qquad Eq. \ 1$$

116 with n_{OH} = 3.10 mmol/g, estimated in a previous study (Brand et al., 2017).

117 **2.3 Emulsion formulation and characterization**

118 **2.3.1 Direct emulsion**

119 The 3 mL aqueous continuous phase was composed of a polymerization system and CNC-

120 Br$_{20\%}$ (ranging from 5 to 25 g/L of dispersed phase). The polymerization system was composed

121 of OEGMA (concentration ranging from 10 wt% to 40 wt% with respect to the aqueous phase),

122 possibly a cross-linker TEGDA (15 mol% compared to the total amount of macromonomer,

123 equivalently 5 wt% compared to the aqueous solution) diluted in salted water (NaCl, 40

124 mmol/L) and the free radical initiator KPS (1 g/100 g (macro)monomer(s)). CNC-Br$_{20\%}$ were

125 dispersed in the polymerization medium using an ultrasonic bath for 2 min and a Bioblock

126 vibra-cell equipped with an ultrasonic tip during 15 s (cycles of 3 s "on" at 20 % power and 3 s

127 "off"). 1 mL of IPM was added to the aqueous suspension and mixed using the ultrasonic tip

128 during 15 s (cycles of 3 s "on" at 30 % power and 3 s "off") to obtain an oil-in-water direct

129 emulsion.

130 Emulsion droplet size distribution was obtained by measuring the diameter of a hundred

131 droplets using ImageJ software processing on optical microscopy images. The droplet surface-

132 average diameter, or Sauter diameter $D_{3,2}$ was calculated as follow (Eq. 2):

133
$$D_{3,2} = \frac{\sum_i N_i D_i^3}{\sum_i N_i D_i^2}$$
Eq. 2

134 Where N_i is the number of droplets with diameter D_i. The standard deviation was also

135 calculated as follow (Eq. 3):

136
$$S = \sqrt{\frac{\sum_1^n (D_i - D_{3,2})^2}{n}}$$
Eq. 3

137 **2.3.2 Double emulsion**

138 The continuous phase was prepared by mixing 3 mL of IPM with CNC-Br$_{90\%}$ (ranging from 5

139 to 20 g/L with respect to the amount of direct emulsion) with an ultrasonic bath for 2 min. 1 mL

140 of the previously described direct emulsion was incorporated to the oil-CNC mixture using a

141 vortex at 1500 rpm for 30 s. The double emulsion drop size was assessed identically as for the

142 direct emulsion using Eq. 2 and Eq. 3. In the following, droplet denomination will refer to the

143 inner emulsion, whereas the term drop will refer to the external one.

144 **2.4 Double emulsion polymerization and characterization**

145 The double emulsions were placed in an oil bath at 75°C for 24h. The emulsion drop size

146 distribution after polymerization was controlled by optical microscopy using Eq. 2 and Eq. 3. A

147 sample of the polymerized double emulsions was then washed with EtOH and dried to assess

148 the morphology by scanning electron microscopy (SEM). In the following, the polymerized

149 double emulsions will be referred as capsules.

150 **2.5 Dye encapsulation within the double emulsion**

151 The hydrophobic dye FY131SC was diluted in IPM to reach a concentration of 0.002 wt%. The

152 hydrophilic dye, toluidine blue, was diluted in salted water (NaCl, 40 mmol/L) to reach a

153 concentration of 0.02 wt%. This solution was used for the (macro)monomer(s) dilution to

154 formulate the stained aqueous phase of the emulsion. The direct emulsion was formulated with

155 the two previously described oil and aqueous phases. This emulsion was then incorporated

into regular IPM to obtain the double emulsion. Both direct and double emulsions were observed using a confocal microscope equipped to assess the effective encapsulation of both dyes.

The encapsulation efficiency (EE) was measured from double emulsions containing only FY131SC in the inner IPM droplets. 500 µL of the continuous supernatant IPM was taken from the double emulsion and diluted in 500 µL of regular IPM. The mixture was then filtered and analyzed by UV-visible spectrophotometry. The EE was calculated as (Eq. 4):

$$\text{Encapsulation efficiency (\%)} = \left(1 - \frac{amount\ of\ dye\ in\ the\ continuous\ phase}{total\ amount\ of\ dye\ in\ the\ double\ emulsion}\right) * 100 \quad \textit{Eq. 4}$$

2.6 Instrumentation

Infrared spectra of unmodified and brominated CNCs were recorded using a Vertex 70 Bruker FT-IR spectrometer. CNC powder was analyzed thanks to an attenuated total reflectance ATR accessory. Each spectrum was recorded between 4000 cm^{-1} and 400 cm^{-1} with a resolution of 4 cm^{-1} with 32 scans.

Optical micrographs were taken on a bright-field upright microscope (Zeiss Axioscope 40) with an Axioscope 105 color camera. Emulsions were placed onto a glass slide, then a spacer was used to avoid compression of the droplets during observation, finally the sample was covered by a lamella. The recorded images were analyzed with ImageJ.

Scanning electron microscopy (SEM) observations were performed with a HITACHI TM-1000 apparatus operating at 15 kV. Samples were coated with a layer of Au-Pd before observation using a plasma at 10 mA for 30 s.

All confocal microscopy images were acquired on a Leica TCS SP5 (Leica Microsystems CMS GmbH, Mannheim, Germany) inverted confocal microscope (DMI6000).

UV-visible spectrophotometry was performed using a Cary 100 UV-vis spectrophotometer between 400 nm and 800 nm, in 500 µL quartz cells.

Contact angles were measured on a Teclis apparatus using the drop deposit technique. Pellets of CNCs were produced from 200 mg of dry material using a 13 mm Evacuable Pellet Die and a manual hydraulic press (5 tons during 1 min). The pellets were kept dry in an oven at 50 °C
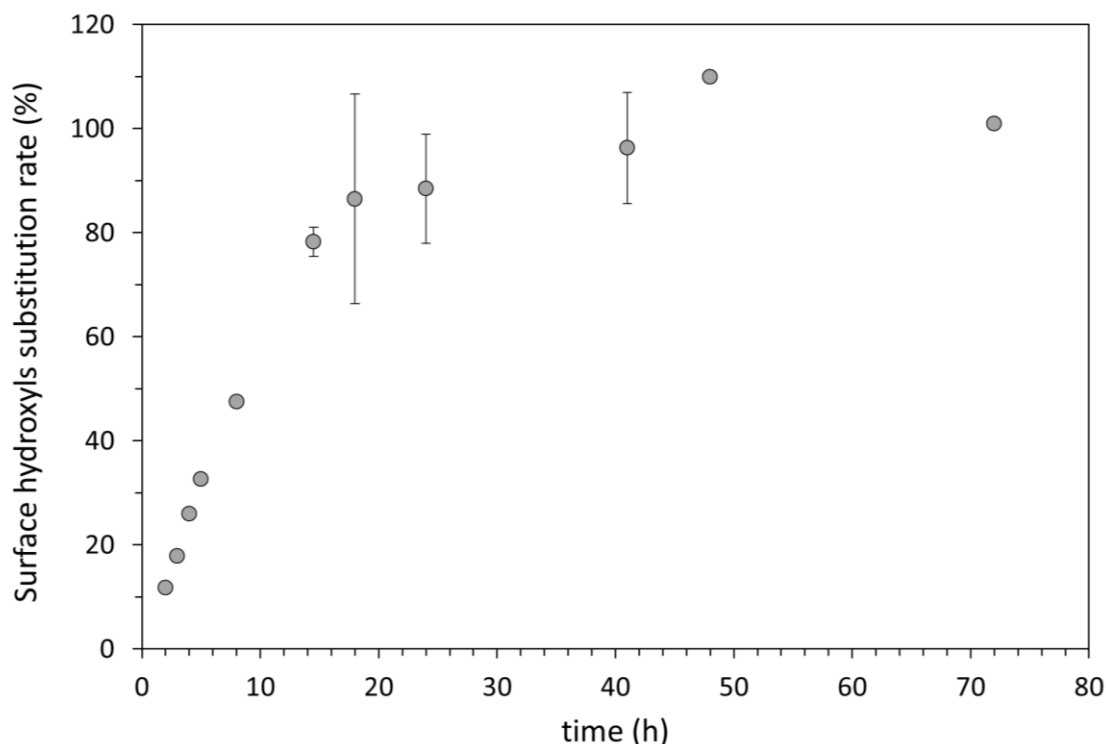
183   prior to experiment. Drops of salted water (4 μL) were deposited on the pellets and the contact

184   angle was measured. For each CNC modification rate, the contact angle was measured at

185   least three times.

186

187   **3. Result and discussion**
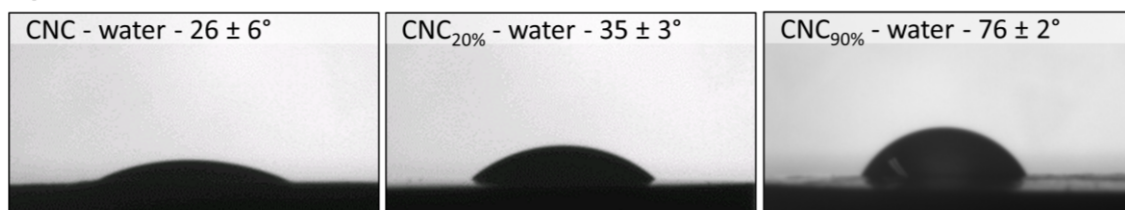
188   **3.1 CNC modification**

189   The CNC were modified using Bibb, enabling the grafting of brominated moieties often used

190   for the initiation of controlled radical polymerization like ATRP, as demonstrated in a previous

191   study (Dupont, Laurichesse, et al., 2021). Here, the grafting was only used in order to increase

192   the overall hydrophobicity of the CNCs. The CNC modification rate of hydroxyl functions into

193   brominated hydrophobic moieties could be controlled by adjusting the reaction time. The more

194   time the reactants were in contact with the CNCs the more hydroxyl functions were esterified,

195   leading to more hydrophobic CNCs. As a consequence, the modification rate functions could

196   be plotted against the reaction time, showing a linear increase in brominated functions followed

197   by a plateau when reaching 100% of hydroxyl substituted by brominated function for at least

198   40 h of reaction (Figure 2A).

Figure 2: A) CNC surface modification rate as a function of the reaction time. Error bars represent the repeatability of the experiment for a given reaction time. B) Characteristics of the two modified CNC batches used in this study. C) Contact angle between water, CNC surfaces and air.

It has been observed that for low modification rates (up to 50%), the CNCs were still hydrophilic enough to be dispersed in water and to stabilize efficiently direct O/W emulsions. Moreover, the surface modification performed on the CNCs enhanced their ability to adsorb at oil-water interfaces, making them more suitable Pickering emulsion stabilizers, compared to pristine crystals. On the contrary, above 50% of modification the CNCs become more hydrophobic and

9

208   can only be dispersed into hydrophobic solvents or oils (Destribats et al., 2014; Finkle et al.,

209   1923). Following Finkle's law, they indeed efficiently stabilize inverse W/O emulsions.

210   In the present study, we chose to work with two sets of surface-modified CNCs, suitable for

211   the stabilization of direct and inverse emulsions. Two batches of CNCs were therefore modified

212   during 3 h and 41 h respectively to reach modification rates of approximately 20% and 90%

213   (Figure 2A, Figure 2B). They are noted CNC-Br$_{20\%}$ and CNC-Br$_{90\%}$ respectively.

214   To further characterize the chemical modification and hydrophilic-lipophilic balance of the

215   CNCs, water contact angles were measured for pristine CNCs and the two CNC-Br batches

216   (Figure 2C). Water droplets were deposited onto the CNC pellets, showing an increase in the

217   contact angle with the increase of brominated moieties. Pristine CNCs exhibited a low contact

218   angle of $26 \pm 6°$ consistent with their intrinsic hydrophilic nature. For low modification rate, the

219   contact angle value increased to $35 \pm 3°$, showing that the CNC-Br$_{20\%}$ are more hydrophobic

220   than their pristine form, but are still quite hydrophilic, as they can be redispersed in water. On

221   the contrary, for high modification rates as for CNC-Br$_{90\%}$, the contact angle increased by 50°

222   compared to pristine particles, up to $76 \pm 2°$, showing the great impact of the surface

223   modification on the hydrophilic/hydrophobic behavior. It is worth noting that this three-phase-

224   contact-angle was measured between CNCs, water and air, which allows a comparison

225   between the different CNCs but does not give the three phase contact angle of the system

226   used in the emulsions: it is therefore useful as a comparative method but does not represent

227   the present system, as the monomer and the oil are missing from this measurement.

228

229   **3.2 Emulsion formulation**

230   **3.2.1 Direct emulsion O/W**

231   Emulsions components were chosen in order to formulate an overall bio-friendly system. IPM

232   was used as oil phase, as a non-toxic biocompatible oil already used in cosmetic and

233   pharmaceutic applications. Regarding the aqueous phase, the polymerization system was

234   selected similarly using biocompatible functionalized polyethylene glycol derivatives, OEGMA

235   and TEGDA. The metastable emulsion was then stabilized using biosourced CNCs.

236   Emulsion formulation parameters were determined based on previous optimization on simple

237   inverse emulsions (Dupont, Laurichesse, et al., 2021). Hence, the concentration of OEGMA

238   was set to 10, 35 or 40 wt% of the aqueous phase, and the possible addition of TEGDA as a

239   cross-linker was set to 15 mol% with regard to the total (macro)monomers concentration (which

240   is equivalent to a composition of 35 wt% of OEGMA and 5 wt% of TEGDA with respect to the

241   aqueous solution). Oil-to-water volume fraction could be tuned, and O/W emulsions were

242   formulated with fraction of 25/75 or 50/50, which will enable later the variation of inner droplets

243   concentration for the double emulsion loading.

244   Stable direct O/W Pickering emulsions were obtained using CNC-Br$_{20\%}$ particles as stabilizers,

245   as they were mainly hydrophilic and could lead to the stabilization of direct emulsion following

246   Finkle's rule (Finkle et al., 1923). The concentration in OEGMA was set to 40 wt%, and the

247   concentration in stabilizing particles was varied from 5 to 25 g/L with respect to the oil phase.

248   The Sauter diameter was measured for each sample and its inverse ($1/D_{3,2}$) was plotted

249   against the CNC-Br$_{20\%}$ concentration (Figure 3).
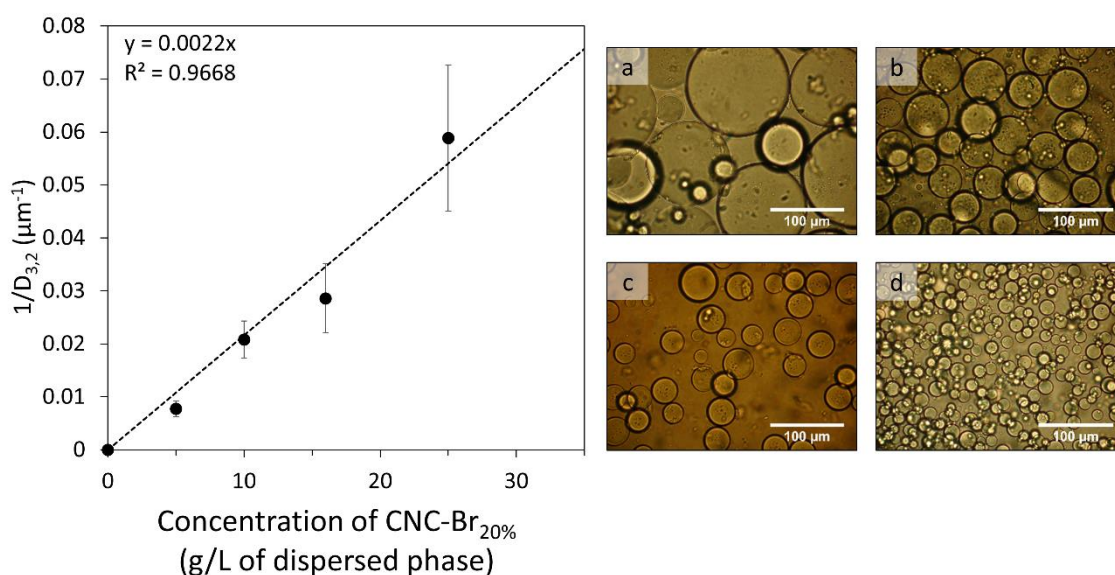
250

251   *Figure 3 : Left, Reverse drop diameter as a function of the amount of CNC-Br$_{20\%}$ in the aqueous phase.*
252   *All the other parameters are kept constant: 25/75$_{V/V}$ of IPM/polymerization system, OEGMA 40 wt% no*
253   *TEGDA. The linear variation highlights the limited coalescence phenomenon occurring in this*
254   *concentration range. Right, optical microscopy shots of the emulsions with a) 5 g/L, b) 10 g/L, c) 16 g/L,*
255   *d) 25 g/L of CNC-Br$_{20\%}$.*

256   The plot shows a linear dependence of the inverse of the diameter with the CNC-Br$_{20\%}$ particle

257   concentration, which is characteristic of the behavior of Pickering emulsions. Indeed, in the

11

258 particle-poor domain, the size can be controlled by the amount of particles thanks to the limited

259 coalescence phenomenon, because of the irreversible adsorption of particles at the oil-water

260 interface (Arditty et al., 2003; Wiley, 1954). From the slope, it is possible to extract the covering

261 ratio (C parameter), which is defined as the proportion of interface covered by particles. The

262 slope is defined as (Schmitt et al., 2014) (Eq. 5):

263
$$\frac{1}{D_{3,2}} = \frac{m_p}{6\rho_p V_d C} \cdot \frac{a_p}{v_p}$$
Eq. 5

264 where a_p and v_p are the projected surface and the volume of the particles in contact with the

265 interface (140x25 nm² and 140x25x25 nm³ respectively, approximating the CNC shape to a

266 parallelepiped rectangle), m_p corresponds to the mass of particles, ρ_p their density (taken as

267 1.6 g/cm³), V_d the volume of the dispersed phase, and C the covering ratio. In the case of

268 CNCs, which can be approximated to parallelepiped particles, a dense monolayer corresponds

269 to a C value of 1. When C>1, the droplets are covered in average by n layers of particles, with

270 C = n x 100 %. Here from the slope, it can be extracted that emulsions droplets are covered

271 by 2 layers of CNCs in average. The formulation of the direct emulsion allows reaching stable

272 emulsions droplets with mean diameters down to 17 µm, which makes them suitable as inner

273 droplets for the double emulsion formulation. Indeed, previous attempts of formulating simple

274 inverse emulsions of the same composition (water phase composed of 40 wt% of OEGMA)

275 enabled producing droplets of average diameter of 400 µm (Dupont, Laurichesse, et al., 2021).

276 It can therefore be assumed that the drops size of the second emulsification will be in the same

277 range and thus suitable for the production of nicely defined double emulsions.

278 **3.2.2 Double emulsion O/W/O**

279 Double emulsions containing the monomers were formulated following a two-step

280 emulsification process, with CNC-Br stabilizing each one of the two interfaces. According to

281 previous characterizations, CNC-Br$_{20\%}$ were used to stabilize the O/W inner emulsion interface,

282 and CNC-Br$_{90\%}$ for the outer interface. The simple direct emulsion was first formulated as

283 described in the section 3.2.1 and used as dispersed phase for the second emulsification. By

284   changing the oil-to-water volume fraction of the direct emulsion, the loading fraction of inner

285   droplets within the double emulsion could be tuned (Eq. 6).

286                          $$n_{inner} = \varphi_{oil} \times \frac{D_{4.3}{}^3}{d_{4.3}{}^3}$$ *Eq. 6*

287   with n_{inner} the average number of inner droplets, φ_{oil} the oil volume fraction of the direct

288   emulsion, $D_{4,3}$ the volume averaged diameter of the external drops and $d_{4,3}$ the volume-

289   averaged diameter of the inner droplets defined as $D_{4,3} = \frac{\sum_i N_i D_i^4}{\sum_i N_i D_i^3}$.

290   Regarding the process, the choice of the second emulsification was determinant as it must not

291   induce the modification, neither fragmentation nor destabilization of the inner emulsion. As a

292   consequence, several mixing procedures were considered, with shear rates lower than the one

293   induced by the ultrasonic probe used for the first emulsification (Ding et al., 2019). Rotor-stator,

294   mechanical stirring and vibrating mixer were tested. In order to assess the stability of the

295   double emulsion, the oil dispersed in the direct emulsion was stained with Nile Red (solubility

296   in water 0.2 mg/mL), and the repartition of the dye after the second emulsification was used

297   as a macroscopic indicator for process viability. More precisely, if the dye was finally present

298   in the continuous phase, then it was assumed that the innermost and outer oily phases have

299   been in contact during the emulsification process. This has to be avoided to prevent dilution of

300   the active to be encapsulated and as a consequence to prevent low encapsulation efficiencies.

301   At the microscopic scale, double emulsions were observed by optical microscopy and the

302   average number of inner droplets was coarsely compared to the theoretical expected value

303   n_{inner} (Eq. 6). Firstly, a rotor-stator Ultra-turrax® emulsification at low power (5000 rpm for 30 s)

304   was employed (Figure 4 a, b). The direct emulsification led to empty double emulsions, similar

305   to inverse emulsions. Therefore, a manual pre-mixing step was added to follow the emulsion

306   evolution step-by-step. After a gentle manual premixing, the external oil was already stained

307   with Nile Red (Figure 4 d), meaning that the emulsification did rupture some of the droplets of

308   the direct emulsion. Regarding the morphology, the effective number of encapsulated inner

309   droplets was already far from the theoretical value of a 250 droplets estimated by Eq. 6. After

310 further stirring using the Ultra-Turrax® rotor–stator mixer, the staining in the continuous oil

311 phase intensified, and no inner droplet was visible anymore (Figure 4 e). Similarly, mechanical

312 stirring ended up in the destabilization of the direct emulsion and an intense coloration was

313 visible in the continuous phase after the second emulsification step (Figure 4 g).
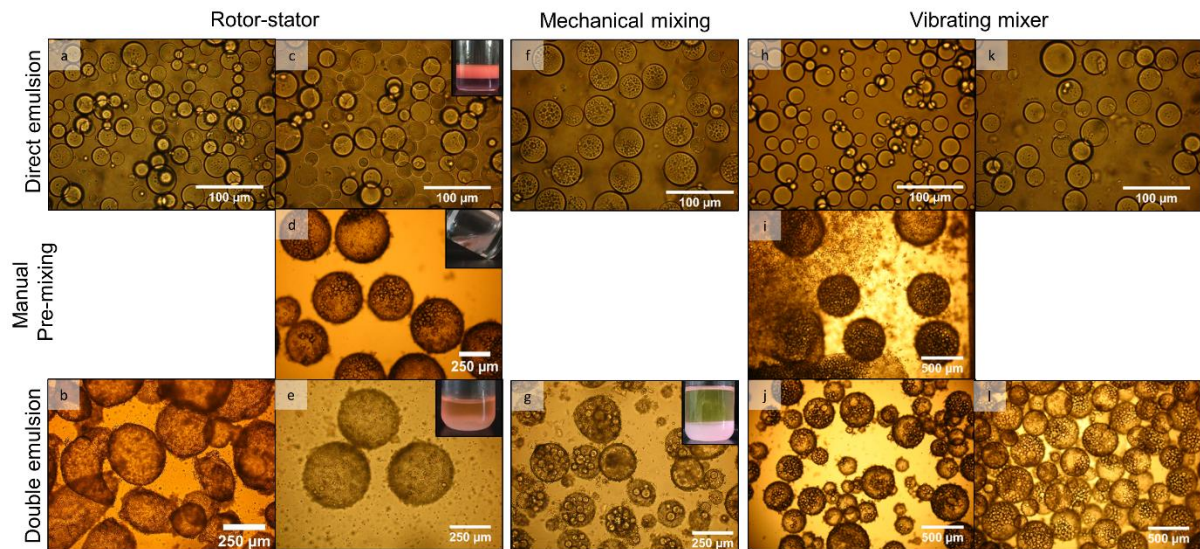
314

315 *Figure 4 : Process optimization for emulsion formulation. a, b) direct and double emulsions from rotor-*
316 *stator mixing. c, d, e) direct, premix and double emulsions from rotor-stator mixing. f,g) direct and double*
317 *emulsions from mechanical stirring. h,i,j) direct, premix and double emulsions from vibrating mixer*
318 *stirring. k,l) direct and double emulsions from vibrating mixer stirring. The inserts, when present, show*
319 *the macroscopic aspect of the emulsion containing Nile Red.*

320 Finally, a gentler process was chosen, and emulsification with a vibrating mixer (1500 rpm for

321 30 s) showed good results upon the double emulsion formulation, provided the suppression of

322 the manual pre-mixing step (Figure 4 l). The inner emulsion average droplet diameter is

323 preserved during the emulsification, as it is equal to 38 ± 7 µm before and 40 ± 7 µm after

324 (Figure 5 left). Moreover, the CNC-Br$_{90\%}$ were efficiently adsorbed at the newly created water-

325 oil interface as no sign of excess particles could be seen in the continuous phase.
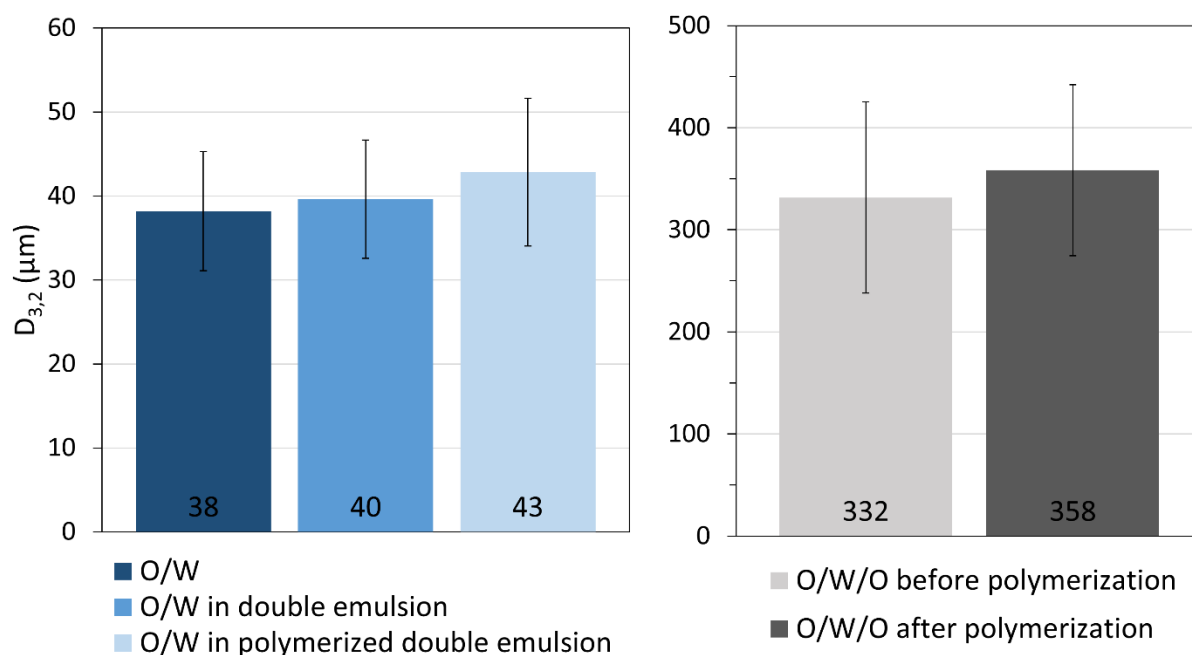
Figure 5: Left) inner droplets size distribution evolution after formulation, after incorporation in the double emulsion and after polymerization of the double emulsion. Right) double emulsion size distribution evolution before and after polymerization. The error bars reflect the drops size distribution width (standard deviation).

By setting the OEGMA concentration to 40 wt% in the aqueous phase, the concentration of CNC-Br$_{90\%}$ was varied and the according diameter of the double emulsion was measured. By plotting the inverse of the drop diameter as a function of the concentration of CNC-Br$_{90\%}$, a linear relationship characteristic of the limited coalescence phenomenon could be evidenced at the drop scale (Figure 6). In a previous contribution (Dupont, Laurichesse, et al., 2021), inverse simple emulsions of a 40 wt% OEGMA solution-in-IPM stabilized by CNC-Br$_{90\%}$ were obtained by homogenization with a rotor-stator, Ultra-turrax® S18N-10G at 15 000 rpm for 30 s. Interestingly, for identical CNC-Br$_{90\%}$ concentrations range, the average emulsion drop diameter was higher for these simple inverse emulsions than for the present double emulsion system (Fig. S2, SI), whereas the opposite was expected since the rotor-stator homogenization is more powerful than the vibrating mixer process. The ability of the CNC to adsorb at the interface is therefore influenced by the presence of the direct inner emulsion and is not only governed by the amount of particles and the power of homogenization. Indeed, in a previous contribution, it has been demonstrated that 41 layers of CNC-Br$_{90\%}$ were present on the inverse

346   emulsions surface (Dupont, Laurichesse, et al., 2021), and in the present case only half this

347   value are adsorbed for each double emulsion drop. This difference could also be influenced

348   by the change in the physical-chemical characteristics such as its viscosity of the dispersed
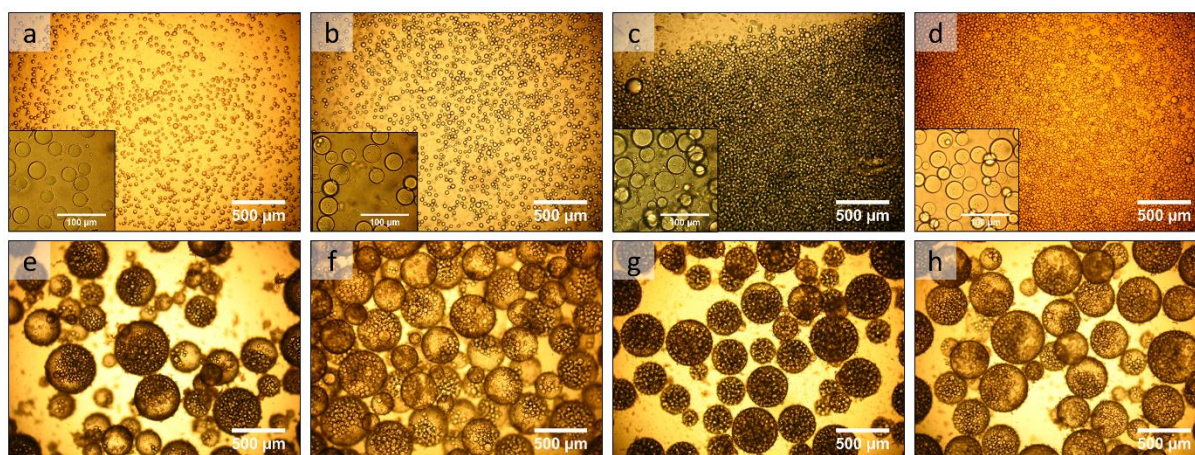
349   phase, for instance.
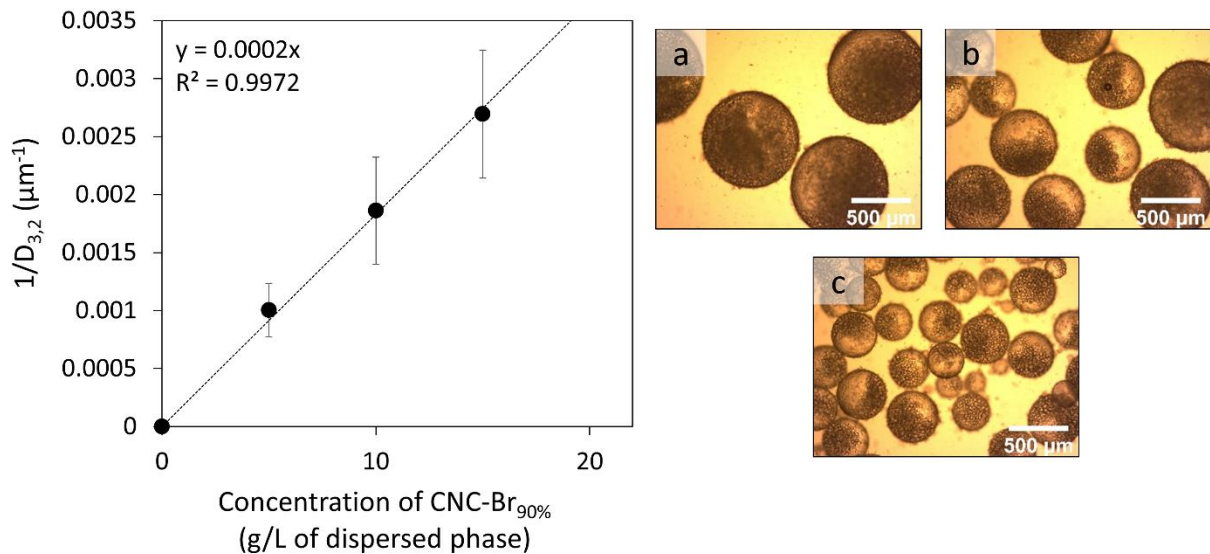
350

351 *Figure 6 : Left, Reverse drop diameter as a function of the amount of CNC-Br$_{90\%}$ in the organic*
352 *continuous phase. All the other parameters are kept constant: 25/75$_{v/v}$ of direct emulsion/IPM, direct*
353 *emulsion IPM/aqueous phase ratio of 25/75$_{v/v}$, OEGMA 40 wt% no TEGDA. The linear variation*
354 *highlights the limited coalescence phenomenon occurring in this concentration range. The error bars*
355 *reflect the drops size distribution width (standard deviation). Right, optical microscopy shots of the*
356 *double emulsions with a) 5 g/L, b) 10 g/L, c) 15 g/L of CNC-Br$_{90\%}$.*

357   Similarly to simple emulsions, a covering ratio could be extracted here from the slope of the

358   linear relationship between the inverse of the drop diameter and the concentration of particles

359   (Figure 6), acknowledging an average of 21 layers of CNC-Br$_{90\%}$ at the drops surface. These

360   multilayers are visible by optical microscopy, but more accurately by SEM (Figure 6, Figure 8),

361   showing a rough solid interface and the presence of CNC aggregates. Regarding the

362   morphology of the double emulsions, optical microscope observation showed that the inner

363   droplets tend to stack at the outer droplet interface (Figure 7B f). This phenomenon can be

364   explained by the van der Waals attractive interactions between the inner droplets and the wall

365   formed by the outer drop surface (Sengupta & Papadopoulos, 1992; Wen et al., 2004). This

366   observation is less visible when increasing the inner droplet volume fraction from 25 vol% to

367   50 vol%. Indeed, as the concentration of inner droplets increases, more volume of the drop is

368   occupied and the segregation becomes less noticeable (Figure 7B g).

369　The aqueous intermediate phase composition could be varied, without disturbing the simple

370　and double emulsion stability (Figure 7A). Stable double emulsions were obtained with

371　different OEGMA concentration of 10 wt% or 40 wt% (Figure 7B a, e and b, f). The addition of

372　TEGDA as a cross-linker to the aqueous solution of OEGMA (concentration of 5 wt% and 35

373　wt% respectively) did not impact neither the direct nor the double emulsion size (Figure 7B d,

374　h, Figure 7A).

|	Inner emulsion O/W volume faction (v/v)	OEGMA (wt%)	TEGDA (wt%)	Inner emulsion diameter (µm)	Double emulsion diameter (µm)
a,e	25/75	10	0	33 ± 8	350 ± 89
b,f	25/75	40	0	35 ± 8	377 ± 107
c,g	50/50	40	0	38 ± 9	332 ± 94
d,h	25/75	35	5	34 ± 9	377 ± 88

375

376　*Figure 7: A) Formulation details of the emulsions presented below. B) Observation by optical microscopy*
377　*of direct simple emulsion, 16 g/L CNC-Br$_{20\%}$, at low oil volume fraction 25/75$_{v/v}$ with varying OEGMA*
378　*concentration a) 10 wt%, b) 40 wt%, c) with high oil volume fraction of 50/50$_{v/v}$, and d) in presence of a*
379　*cross-linker (OEGMA/TEGDA 35/5 wt%). e-h) Respective double emulsions formulated with 20 g/L of*
380　*CNC-Br$_{90\%}$.*

381

3.3 Emulsion polymerization

383　Double emulsions were formulated with varying concentrations of OEGMA and TEGDA in the

384　aqueous phase (10 wt%, 35 wt%-5wt%, 40wt%) and with two different loading fractions of

385　inner droplets (25 vol% n_{inner}~250, 50 vol% n_{inner}~500). They were further polymerized by

386　immersion in an oil bath at 75°C for 24 h. After polymerization, the emulsions were still

387　dispersible in the supernatant IPM, contrary to observation of OEGMA/TEGDA polymerized

388　emulsions initially stabilized by surfactants, which could only be redispersed in an aqueous

389　medium (Stasse et al., 2020). Optical microscope observation showed a good stability of the

390   double emulsions upon heating and polymerization as the spherical morphology (Figure 8) and

391   the mean diameters of both inner droplets and outer drops were preserved (Figure 5). Both

392   internal droplets and external drops kept their average size distribution meaning that no

393   coalescence nor destabilization events occurred during the polymerization process. For low

394   loading fraction of inner droplets, the sticking phenomenon observed on non-polymerized

395   double emulsions is even more visible after polymerization, with a clear segregation of the

396   inner droplets on one side of the double emulsion, resulting in "Janus-like" polymer beads

397   (Figure 8 a, b, d). The phenomenon induced by the van der Waals attractive interactions was

398   most certainly enhanced by the creaming of the oil droplets within the drops during the 24h of

399   polymerization, which were performed without mixing. Morphologies were further

400   characterized by SEM, to assess the behavior of the capsules under a dry state and under

401   vacuum (Figure 8 e-h). As it was previously observed for polymerized inverse emulsions

402   (Dupont, Laurichesse, et al., 2021), the polymerized double emulsions presented on their

403   surface a dense cover of CNCs, which might participate in the good redispersibility of the

404   emulsions in IPM after polymerization. Almost all capsules could withstand the vacuum of the

405   SEM chamber (10^{-5} Pa) without collapsing, except for the lowest OEGMA concentration (10

406   wt%), most certainly because of the low filling in polymer inside the aqueous core (Figure 8 e).

407   For higher concentration in macromonomer, the objects kept their spherical shape with no

408   deformation induced by the vacuum. The capsules were hand-cut to inspect their inner core.

409   As expected, matrix morphology was observed, with visible cavities assessing for the presence

410   of the oil inner droplets (Figure 8 f, g, h). For low loading fractions of inner droplets about 25

411   vol% (Figure 8 f, g), the repartition of the cavities is clearly segmented with one part of the

412   capsule composed of full polymer and the other side concentrating the cavities made from the

413   presence of inner oil droplets. The increase in the inner droplet loading fraction from 25 vol%

414   to 50 vol% (Figure 8 g) is visible with an increase in the average number of cavities per capsule,

415   but also from the more even repartition of the cavities within the capsule, less subjected to the

416   microscopic segregation due to the van der Waals interactions.
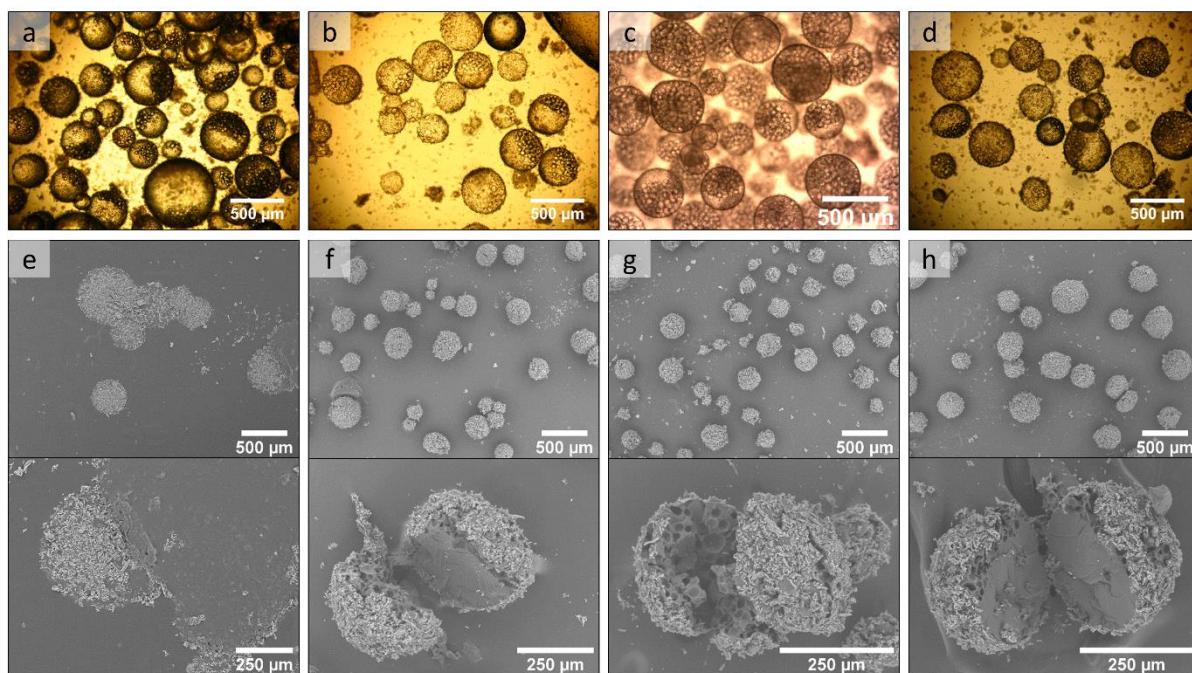
Figure 8: Optical microscopy images of polymerized emulsions with 25 %v inner oil and a) 10 wt% OEGMA, b) 40 wt% OEGMA, d) 35 wt% OEGMA and 5 wt% TEGDA, and c) with 50 %v inner oil and 40 wt% OEGMA. e-h) SEM pictures of the respective polymerized double emulsions, from a low and high magnification.

3.4 Encapsulation efficiency

Double emulsions of OEGMA and TEGDA were efficiently stabilized by CNCs and further polymerized to obtain well-defined solid capsules. To increase the impact of these objects, their encapsulation ability was assessed as a proof of concept. The choice of encapsulated species was orientated towards fluorescent dyes (as models) which can be easily followed visually by confocal microscopy and quantified by UV-Vis spectrophotometry. The hydrophobic dye FY131SC, which is composed of "Solvent Red 175" dye, was chosen because of its very low solubility in water, with a maximum of absorption at 530 nm (full absorbance spectrum Fig. S3, SI). Its addition to IPM did not impact the emulsion formulation (Figure 9 a, b), since both droplets and drops average diameter were equal to 47 ± 8 µm and 367 ± 103 µm respectively without dye and to 38 ± 9 µm, 332 ± 94 µm respectively in presence of FY131SC. The choice of the hydrophilic dye was subjected to optimization as it should have a different range of maximum of absorption and emission than the hydrophobic one, but also should not present interfacial properties in order not to interfere with the emulsion formulation. Therefore, toluidine

19

blue was preferred since it did not induce any change in the double emulsion formulation (Figure 9 c, d), contrary to other dyes like methylene blue which contributed in increasing the direct emulsion droplet diameter (Fig. S4, SI).
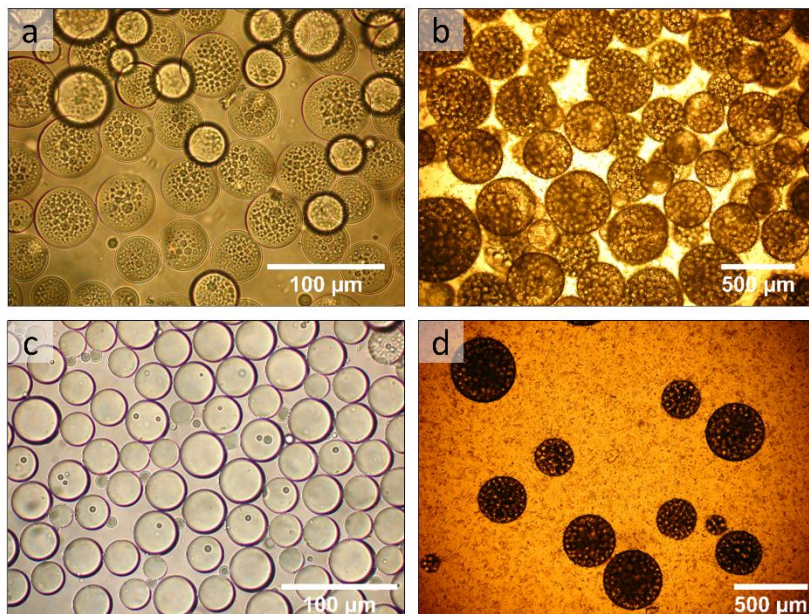
Figure 9: Optical microscopy picture of direct (a,c) and corresponding double emulsion (b,d) in presence of a, b) FY131SC and c, d) both FY131SC and toluidine blue.

Confocal microscopy observation was performed on the stabilized double emulsion to verify the effectiveness of the encapsulation and the special repartition of both dyes. Emulsions were imaged by transmitted light and by fluorescence on a medium plane to enable the visualization of the inner droplets. Each dye was imaged on a separate channel (hydrophobic FY131SC appears in green and hydrophilic toluidine blue appears in red) and both signals were merged by computation. The experiment shows that both toluidine blue and FY131SC are present in the aqueous and oil phase of the direct emulsion respectively (Figure 10 i). For the double emulsion, the inner droplets can be easily distinguished from the intermediate polymerized phase as they are selectively labelled by the hydrophobic dye (Figure 10 g). The polymer phase, which appears red is also selectively stained by the hydrophilic dye (Figure 10 f). Another feature which might be of interest to notice is the light green staining in the background assessing for the presence of the hydrophobic dye in the continuous phase, and indicating the occurrence of leakage following the second emulsification. However, as the fluorescence intensity in the background is low compared to the inner droplets, the concentration of dye in

457 the continuous phase can be considered as low and therefore that the leakage is not too

458 pronounced.

459
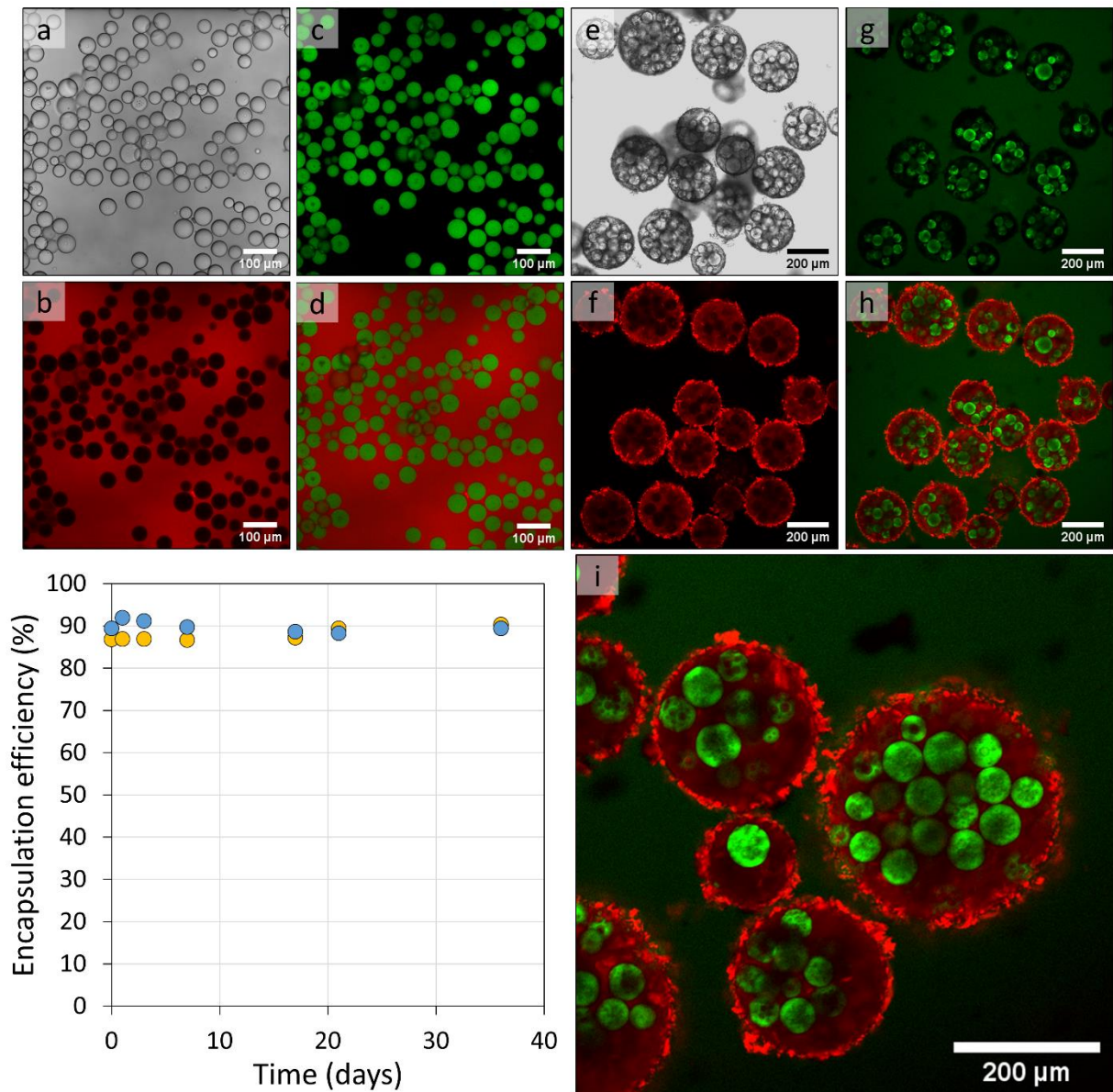
*Figure 10: Pictures – Confocal microscopy image of a direct emulsion with toluidine blue and FY131SC,
a) in bright field, b) red channel, c) green channel and d) superimposition of the red and green channels.
Toluidine blue and FY131SC are revealed by the red and green channels respectively. e-h) Resulting
double emulsion with toluidine blue and FY131SC, and i) close-up at higher magnification. Images were
taken at a given z. Graph – Encapsulation efficiency of double emulsions of OEGMA and TEGDA, with
(blue) and without (yellow) polymerization. The point at t = 0 corresponds to the sample right after
formulation, and t = 1 day corresponds to the sample after 24h of polymerization for the blue curve.*

467 In order to corroborate this hypothesis, and quantify the amount of dye that could effectively

468 be encapsulated within the double emulsion-templated capsules, indirect encapsulation

469 efficiency measurement was performed. Double emulsions with FY131SC in the inner oil

470 droplets were formulated with 35 wt% OEGMA and 5 wt% TEGDA in the intermediate phase.

471   One double emulsion was kept at ambient temperature as a control experiment, while the other

472   was polymerized at 75°C for 24h. The presence of dye in the IPM continuous phase was

473   measured over time by UV-Visible spectrophotometry. Thanks to Eq. 4, the encapsulation

474   efficiency was calculated for both non-polymerized and polymerized double emulsions. Both

475   double emulsions showed good encapsulation efficiency of about 90% directly after

476   formulation (Figure 10). After polymerization, almost no dye could be detected into the

477   continuous phase, giving an estimated encapsulation efficiency of about 90% (Figure 10, blue).

478   A control experiment has been additionally performed, and has shown that the hydrophobic

479   dye does not degrade when submitted to 75°C during 24h (Figure S5, SI). Hence, the absence

480   of dye detection into the continuous phase can be accurately linked to the good encapsulation

481   efficiency and not to a dye leakage followed by degradation. This encapsulation efficiency

482   value remained constant over a month, for both the non-polymerized and the polymerized

483   double emulsions. Hence, the polymerization process of the double emulsion, even in harsh

484   conditions of temperature, did not affect neither the stability of the system nor the

485   encapsulation efficiency of the hydrophobic dye, which is promising regarding active-delivery

486   applications.

487

488   **4. Conclusion**

489   We have shown that O/W/O double emulsions could be stabilized using solely brominated

490   cellulose nanocrystals. Their modification rate was directly linked to the reaction time, and

491   monitors the ability of the particles to stabilize either direct or inverse emulsion. Double

492   emulsion could be formulated using two batches of CNCs, one with a low modification rate

493   about 20% and the other with a high modification rate of 90%. Isopropyl myristate, a polar

494   biocompatible oil was used as inner oil phase and as continuous medium. The aqueous

495   intermediate phase was composed of oligoethylene glycol derivatives, namely hydroxyl

496   oligoethylene glycol methacrylate and tertraethylene glycol diacrylate. For the first time, a

497   double emulsion stabilized solely by CNCs was polymerized. The aqueous intermediate phase

498   was polymerized by free radical polymerization, and led to solid matrix capsules, which

499   conserved the initial emulsion characteristics, with tunable inner droplets content, and varying

500   monomer(s) fraction. Finally, their use as double encapsulation vessels was investigated. Both

501   hydrophobic and hydrophilic dyes could be encapsulated within the inner droplets and the

502   intermediate phase respectively. The encapsulation efficiency of the hydrophilic dye was equal

503   to 100% given the insolubility of the dye in the other phases. For the hydrophobic dye, it was

504   measured approximately equal to 90% indicating promising results to further extend their

505   application to controlled delivery.

506

512 **References**

513 Arditty, S, Whitby, C. P., Binks, B. P., Schmitt, V., & Leal-Calderon, F. (2003). Some general

514   features of limited coalescence in solid-stabilized emulsions. *Eur. Phys. J. E*, *11*, 273–

515   281. https://doi.org/10.1140/epje/i2003-10018-6

516 Arditty, Stéphane, Schmitt, V., Giermanska-Kahn, J., & Leal-Calderon, F. (2004). Materials

517   based on solid-stabilized emulsions. *Journal of Colloid and Interface Science*, *275*, 659–

518   664. https://doi.org/10.1016/j.jcis.2004.03.001

519 Brand, J., Pecastaings, G., & Sèbe, G. (2017). A versatile method for the surface tailoring of

520   cellulose nanocrystal building blocks by acylation with functional vinyl esters.

521   *Carbohydrate Polymers*, *169*, 189–197. https://doi.org/10.1016/j.carbpol.2017.03.077

522 Cunha, A. G., Mougel, J.-B., Cathala, B., Berglund, L. A., & Capron, I. (2014). Preparation of

523   double Pickering emulsions stabilized by chemically tailored nanocelluloses. In

524   *Langmuir* (Vol. 30). https://doi.org/10.1021/la5017577

525 Deng, Z., Jung, J., Simonsen, J., & Zhao, Y. (2018). Cellulose nanocrystals Pickering

526   emulsion incorporated chitosan coatings for improving storability of postharvest Bartlett

527   pears (Pyrus communis) during long-term cold storage. *Food Hydrocolloids*, *84*, 229–

528   237. https://doi.org/10.1016/J.FOODHYD.2018.06.012

529 Destribats, M., Gineste, S., Laurichesse, E., Tanner, H., Leal-Calderon, F., Héroguez, V., &

530   Schmitt, V. (2014). Pickering Emulsions: What Are the Main Parameters Determining

531   the Emulsion Type and Interfacial Properties? *Langmuir*, *30*, 9313–9326.

532   https://doi.org/10.1021/la501299u

533 Ding, S., Serra, C. A., Vandamme, T. F., Yu, W., & Anton, N. (2019). Double emulsions

534   prepared by two–step emulsification: History, state-of-the-art and perspective. In *Journal*

535   *of Controlled Release* (Vol. 295, pp. 31–49). Elsevier B.V.

536   https://doi.org/10.1016/j.jconrel.2018.12.037

537 Dupont, H., Fouché, C., Dourges, M.-A., Schmitt, V., & Héroguez, V. (2020). Polymerization

538   of cellulose nanocrystals-based Pickering HIPE towards green porous materials.

539   *Carbohydrate Polymers*, *243*, 116411. https://doi.org/10.1016/j.carbpol.2020.116411

540   Dupont, H., Laurichesse, E., Héroguez, V., & Schmitt, V. (2021). Green Hydrophilic Capsules

541   from Cellulose Nanocrystal-Stabilized Pickering Emulsion Polymerization: Morphology

542   Control and Spongelike Behavior. *Biomacromolecules*, *22*(8), 3497–3509.

543   https://doi.org/10.1021/acs.biomac.1c00581

544   Dupont, H., Maingret, V., Schmitt, V., & Héroguez, V. (2021). New Insights into the

545   Formulation and Polymerization of Pickering Emulsions Stabilized by Natural Organic

546   Particles. *Macromolecules*, *54*(11), 4945–4970.

547   https://doi.org/10.1021/acs.macromol.1c00225

548   Finkle, P., Draper, H. D., & Hildebrand, J. H. (1923). The Theory of Emulsification. *Journal of*

549   *American Chemical Society*, *45*(12), 2780–2788. https://pubs.acs.org/sharingguidelines

550   Gestranius, M., Stenius, P., Kontturi, E., Sjöblom, J., & Tammelin, T. (2017). Phase

551   behaviour and droplet size of oil-in-water Pickering emulsions stabilised with plant-

552   derived nanocellulosic materials. *Colloids and Surfaces A: Physicochemical and*

553   *Engineering Aspects*, *519*, 60–70. https://doi.org/10.1016/j.colsurfa.2016.04.025

554   Gonzalez Ortiz, D., Pochat-Bohatier, C., Cambedouzou, J., Bechelany, M., & Miele, P.

555   (2020). Current Trends in Pickering Emulsions: Particle Morphology and Applications.

556   *Engineering*. https://doi.org/10.1016/j.eng.2019.08.017

557   Guo, J., Du, W., Gao, Y., Cao, Y., & Yin, Y. (2017). Cellulose nanocrystals as water-in-oil

558   Pickering emulsifiers via intercalative modification. *Colloids and Surfaces A:*

559   *Physicochemical and Engineering Aspects*, *529*, 634–642.

560   https://doi.org/10.1016/j.colsurfa.2017.06.056

561   Hedjazi, S., & Razavi, S. H. (2018). A comparison of Canthaxanthine Pickering emulsions,

562   stabilized with cellulose nanocrystals of different origins. *International Journal of*

563   *Biological Macromolecules*, *106*, 489–497.

564   https://doi.org/10.1016/j.ijbiomac.2017.08.030

565   Kalashnikova, I., Bizot, H., Cathala, B., & Capron, I. (2011). New Pickering Emulsions

566   Stabilized by Bacterial Cellulose Nanocrystals. *Langmuir*, *27*(12), 7471–7479.

567   https://doi.org/10.1021/la200971f

568 Lee, K.-Y., Blaker, J. J., Murakami, R., Heng, J. Y. Y., & Bismarck, A. (2013). *Phase*

569 *Behavior of Medium and High Internal Phase Water-in-Oil Emulsions Stabilized Solely*

570 *by Hydrophobized Bacterial Cellulose Nanofibrils.* https://doi.org/10.1021/la4032514

571 Mackie, A., Gourcy, S., Rigby, N., Moffat, J., Capron, I., & Bajka, B. (2019). The fate of

572 cellulose nanocrystal stabilised emulsions after simulated gastrointestinal digestion and

573 exposure to intestinal mucosa †. *Nanoscale, 11.* https://doi.org/10.1039/c8nr05860a

574 Matos, M., Timgren, A., Sjöö, M., Dejmek, P., & Rayner, M. (2013). Preparation and

575 encapsulation properties of double Pickering emulsions stabilized by quinoa starch

576 granules. *Colloids and Surfaces A: Physicochemical and Engineering Aspects, 423,*

577 147–153. https://doi.org/10.1016/j.colsurfa.2013.01.060

578 Meng, T., Gao, X., Zhang, J., Yuan, J., Zhang, Y., & He, J. (2008). Graft copolymers

579 prepared by atom transfer radical polymerization (ATRP) from cellulose. *Polymer, 50,*

580 447–454. https://doi.org/10.1016/j.polymer.2008.11.011

581 Morandi, G., Heath, L., & Thielemans, W. (2009). Cellulose Nanocrystals Grafted with

582 Polystyrene Chains through Surface Initiated Atom Transfer Radical Polymerization (SI-

583 ATRP). *Langmuir, 25*(14), 5. https://doi.org/10.1021/la900452a

584 Pan, J., Yin, Y., Gan, M., Meng, M., Dai, X., Wu, R., Shi, W., & Yan, Y. (2015). Fabrication

585 and evaluation of molecularly imprinted multi-hollow microspheres adsorbents with

586 tunable inner pore structures derived from templating Pickering double emulsions.

587 *Chemical Engineering Journal, 266,* 299–308.

588 https://doi.org/10.1016/J.CEJ.2014.11.126

589 Pickering, S. U. (1907). CXCVI.—Emulsions. *Journal of the Chemical Society, Transactions,*

590 *91,* 2001–2021.

591 Ramsden, W. (1904). Separation of solids in the surface-layers of solutions and

592 'suspensions' (observations on surface-membranes, bubbles, emulsions, and

593 mechanical coagulation).—Preliminary account. *Proceedings of the Royal Society of*

594 *London, 72 (477-48,* 156–164.

595 Sarkar, A., & Dickinson, E. (2020). Sustainable food-grade Pickering emulsions stabilized by

596   plant-based particles. *Current Opinion in Colloid & Interface Science*, *49*, 69–81.

597   https://doi.org/10.1016/j.cocis.2020.04.004

598 Schmitt, V., Destribats, M., & Backov, R. (2014). Colloidal particles as liquid dispersion

599   stabilizer: Pickering emulsions and materials thereof. *Comptes Rendus Physique*, *15*(8–

600   9), 761–774. https://doi.org/10.1016/j.crhy.2014.09.010

601 Sengupta, A. K., & Papadopoulos, K. D. (1992). van der Waals Interaction between a Colloid

602   and the Wall of Its Host Spherical Cavity. *Journal of Colloid and Interface Science*,

603   *152*(2), 534–542.

604 Spyropoulos, F., Duffus, L. J., Smith, P., & Norton, I. T. (2019). Impact of Pickering

605   Intervention on the Stability of W1/O/W2 Double Emulsions of Relevance to Foods.

606   *Langmuir*, *35*, 15137–15150. https://doi.org/10.1021/acs.langmuir.9b01995

607 Stasse, M., Laurichesse, E., Vandroux, M., Ribaut, T., Héroguez, V., & Schmitt, V. (2020).

608   Cross-linking of double oil-in-water-in-oil emulsions: A new way for fragrance

609   encapsulation with tunable sustained release. *Colloids and Surfaces A:*

610   *Physicochemical and Engineering Aspects*, *607*, 125448.

611   https://doi.org/10.1016/j.colsurfa.2020.125448

612 Wen, L., Cheng, J., Zou, H., Zhang, L., Chen, J., & Papadopoulos, K. D. (2004). van der

613   Waals Interaction between Internal Aqueous Droplets and the External Aqueous Phase

614   in Double Emulsions. *Langmuir*, *20*, 8391–8397. https://doi.org/10.1021/la049353s

615 Werner, A., Schmitt, V., Sèbe, G., & Héroguez, V. (2019). Convenient Synthesis of Hybrid

616   Polymer Materials by AGET-ATRP Polymerization of Pickering Emulsions Stabilized by

617   Cellulose Nanocrystals Grafted with Reactive Moieties. *Biomacromolecules*, *20*(1), 490.

618   https://doi.org/10.1021/acs.biomac.8b01482

619 Wiley, R. M. (1954). Limited coalescence of oil droplets in coarse oil-in-water emulsions.

620   *Journal of Colloid Science*, *9*(5), 427–437. https://doi.org/10.1016/0095-8522(54)90030-

621   6

622 Zhang, Z., Tam, K. C., Wang, X., & Sèbe, G. (2018). Inverse Pickering Emulsions Stabilized

623   by Cinnamate Modified Cellulose Nanocrystals as Templates to Prepare Silica

624   Colloidosomes. *ACS Sustainable Chemistry and Engineering, 6*(2), 2583–2590.

625   https://doi.org/10.1021/acssuschemeng.7b04061

626